Editors' Suggestion | Featured in Physics

Discrete Electronic Subbands due to Bragg Scattering at Molecular Edges

A. Martín-Jiménez,[1] J. M. Gallego,[2] R. Miranda,[3,1] and R. Otero[3,1,*]
[1]Instituto Madrileño de Estudios Avanzados en Nanociencia (IMDEA-NANO), 28049 Madrid, Spain
[2]Instituto de Ciencia de Materiales de Madrid (ICMM-CSIC), 28049 Madrid, Spain
[3]Departamento de Física de la Materia Condensada and Condensed Matter Physics Center (IFIMAC), Universidad Autónoma de Madrid, 28049 Madrid, Spain

(Received 8 October 2018; published 30 April 2019)

The discretization of the electronic structure of nanometer-size solid systems due to quantum confinement and the concomitant modification of their physical properties is one of the cornerstones for the development of nanoscience and nanotechnology. In this Letter we demonstrate that the Bragg scattering of Cu(111) surface-state electrons by the periodic arrangement of tetracyanoquinodimethane molecules at the edges of self-assembled molecular islands, along with the dominant contribution of backscattering processes to the electronic density of states, discretizes the possible values of the electron momentum parallel to the island edge. The electronic structure consists thus of a discrete number of subbands which occur in a nonclosed space, and therefore without quantum confinement.

DOI: 10.1103/PhysRevLett.122.176801

The discretization of the electronic energy levels upon confinement in regions smaller than their coherence length is a fundamental result of quantum mechanics [1] that determines the electronic structure of solid-state nanostructures. It is a key ingredient to understanding phenomena as diverse as the optical and transport properties of semiconductor quantum dots, wires, and wells [2]; the oscillatory behavior of the superconducting transition temperature in thin films [3]; the thermal stability of metallic thin films [4–7]; the magnetic coupling across thin nonmagnetic spacers [8,9]; etc. In solid-state nanostructures, confinement in one direction is achieved by reflection of the electronic wave function at two different interfaces. In the absence of any other discretization mechanism, one single confining interface is not enough to obtain a discrete subband structure: reflection at the interface would simply preserve $k_{\parallel}$ and reverse $k_{\perp}$, and the interference between incoming and outgoing electrons would lead to electron standing waves with a continuous range of momenta [10–14].

In this Letter, we show low-temperature scanning tunneling microscopy and spectroscopy results demonstrating that the electronic structure of the two-dimensional electron gas (2DEG) at the Cu(111) surface near the edges of self-assembled tetracyanoquinodimethane (TCNQ) islands consists of a discrete set of subbands corresponding to a discrete set of $k_{\parallel,n}$ values even when other confining interfaces are much farther apart than the electron's coherence length (of the order of 40 nm in Cu(111) [14]). The values of $k_{\parallel,n}$ are equally spaced by an amount $G/2$, where $G = 2\pi/a$ is the reciprocal lattice vector corresponding to the periodicity a of the molecular edge. Our analysis reveals that this effect arises from coherent Bragg diffraction of surface-state electrons in backscattering configuration. To our knowledge, this is the first example in which the discretization of the electronic structure around solid-state nanostructures is not caused by electron confinement but by diffraction, leading to a 2D periodic perturbation of the charge density and density of states (DOS) of the surface surrounding molecular islands with potentially important implications for the adsorption and reaction of further adsorbates.

The experiments were carried out in an ultrahigh vacuum (UHV) chamber ($P \sim 10^{-10}$ Torr) equipped with an omicron low-temperature scanning tunneling microscope (LT-STM) and facilities for sample cleaning and evaporation of organic material. Clean Cu(111) surfaces with large terraces were obtained by sputtering the sample with Ar^+ ions ($P_{Ar} \sim 10^{-5}$ Torr, 1.5 keV) followed by annealing to 500 K for 10 minutes. TCNQ molecules were deposited from a molecular evaporator (sublimation temperature 360 K) with the substrate held at RT. $dI/dV(E)$ were recorded with a lock-in amplifier using a modulation voltage of 10–20 mV under open feedback conditions. For recording $dI/dV(x,E)|_y$ as a function of the position x along specific lines in the sample, the feedback loop was closed before moving from one point to the next. $dI/dV(x,y)|_E$ maps at specific energies were measured under closed feedback loop conditions.

As previously reported [15,16], TCNQ molecules self-assemble onto the Cu(111) surface with a rhomboidal unit cell of size 4.8 nm × 1.8 nm [long diagonal × short diagonal, Fig. 1(a)]. The islands tend to be elongated along the direction of the short diagonal of the unit cell, and the island edges in this direction follow straight lines with a rather small number of defects [Fig. 1(a)]. The molecular

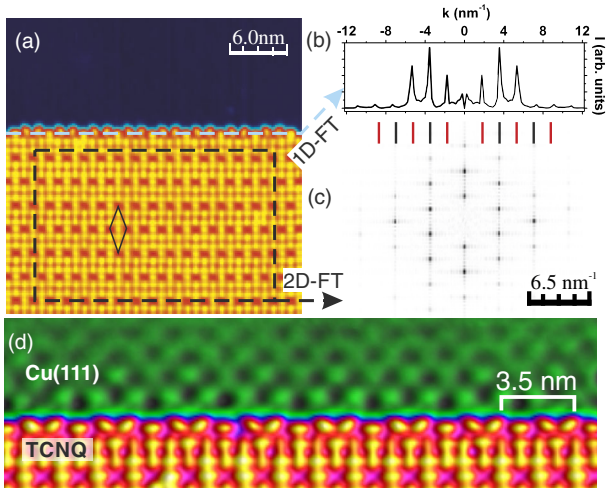

FIG. 1. (a) STM image (30.2×30.2 nm^2, $V_{\mathrm{bias}} = 1.4$ V, $I_t = 150$ pA) of the edge of a TCNQ island, showing the bulk and edge molecular arrangements. The rhomboidal unit cell is shown. (b) 1D Fourier transform (FT) of a scan line over the island edge. (c) 2D FT of the island bulk. Black tick marks correspond to the peaks in the 1D FT that correspond to the projection of the bulk reciprocal space over the edge direction, while red ticks mark the position of the new peaks due to the edge periodicity. (d) STM image (26.3×8.6 nm^2, $I_t = 150$ pA) recorded at low voltage ($V_{\mathrm{bias}} = 100$ meV), where the standing wave pattern of the Cu(111) surface state is visible.

structure at these edges is not simply the crystal termination of the 2D self-assembled structure: a 1D reconstruction of the island edge takes place, with a periodicity of 3.5 nm, which is twice the size of the short rhombus diagonal [see Figs. 1(a), 1(b), and 1(c)]. STM images recorded at low voltages (<100 mV, which are sensitive to the density of states at the Fermi level) close to the reconstructed island edge reveal the standing wave pattern caused by interference between incoming and scattered electrons [Fig. 1(d)]. Standing waves surrounding individual molecular adsorbates [17] or arrays or organic molecules [18–20] have been previously found, but in previous studies (both for organic adsorbates or other types of 0 and 1D defects [10–13]) the wave fronts follow 1D continuous curves on the surface, instead of a 2D array of maxima and minima like the one in Fig. 1(d).

In order to investigate this peculiar standing wave pattern, we have recorded $dI/dV(x, E)$ spectra on the bare Cu(111) surface at different distances x from the TCNQ edges [Fig. 2(e)] and also close to monatomic step edges on a clean Cu(111) surface [Fig. 2(a)]. In both cases, the spectra reveal the onset of conductivity at about 0.45 eV below the Fermi level, characteristic of the Cu(111) surface state. For higher energies, the conductivity oscillates with the distance to the linear scatterer, with a period that decreases with increasing energies. The most striking difference between the scattering at TCNQ edges and at bare Cu(111) steps is in the dependence of the amplitude

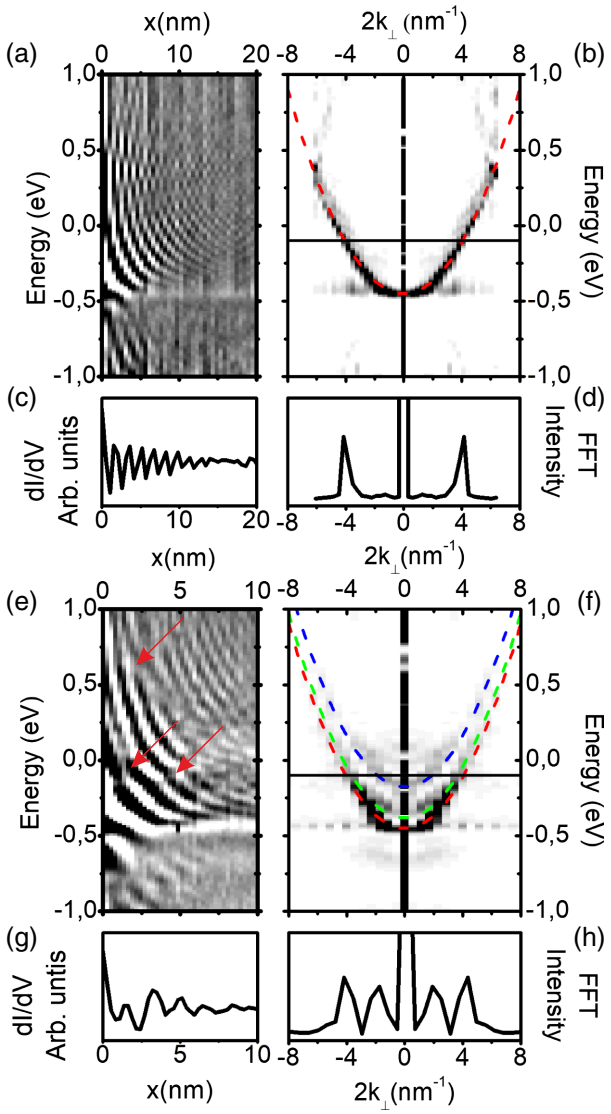

FIG. 2. (a) $dI/dV(x, E)$ measured along the perpendicular direction of a bare step edge ($V_{\mathrm{bias}} = 1.4$ V, $I_t = 1.4$ nA, $V_{\mathrm{mod}} = 14$ mV, length of the line 20 nm). (b) FFT of the data of (a), revealing the existence of only one band. (c) Cut of (a) for a bias voltage of -100 mV. (d) Cut of (b) for a bias voltage of -100 meV. (e) $dI/dV(x, E)$ measured on bare Cu(111) along the edge perpendicular to the TCNQ island ($V_{\mathrm{bias}} = 1.4$ V, $I_t = 1.4$ nA, $V_{\mathrm{mod}} = 14$ mV, length of the line 10 nm). (f) FFT of the data of (e), revealing the existence of three subbands. (g) Cut of (e) for a bias voltage of -100 mV. (h) Cut of (f) for a bias voltage of -100 meV.

on the distance: while for bare monatomic steps the intensity decreases monotonically with the distance to the step [Fig. 2(c)], as previously reported [10,11,14], for TCNQ edges there is an additional amplitude modulation [Fig. 2(g)]. Also, while the distance at which a particular wave front is found for scattering with a copper step edge increases smoothly with decreasing energies, for scattering with TCNQ island edges the evolution presents well-defined kinks or discontinuities, marked by red arrows

in Fig. 2(e). Both phenomena can be attributed to the superposition of waves with different wavelengths. This is more clearly seen by performing a line-by-line Fourier transform (FT) of the experimental data at each energy, showing the tunneling conductance as a function of $\Delta k_\perp = 2k_\perp$ and E [Figs. 2(b) and 2(f)]. For scattering with a bare Cu(111) step, only one wave vector is found to contribute at each energy above the surface-state onset [Fig. 2(d)], with the parabolic dispersion relation of the surface state [solid red line in Fig. 2(b)]. On the other hand, for scattering with the TCNQ edge, alongside the band originating from the normal reflection of surface-state electrons, two other parabolas are clearly visible at higher energies [Fig. 2(f)]. The bottoms of the new bands are shifted upwards with respect to the surface-state onset by 70 and 270 meV, respectively, but the effective mass does not change significantly [blue and green curves in Fig. 2(d)]. The electronic structure of the 2DEG near a single edge of the molecular islands thus consists of a discrete series of electronic subbands which disperse parabolically with $k_\perp$, even when a second edge is not present to produce confinement.

The origin of the discrete subband structure can be understood by examining the standing wave patterns on the copper surface close to the molecular islands in $dI/dV(x,y)|_E$ maps at different bias voltages [Figs. 3(a), 3(c), and 3(e)]. The wave vectors that contribute to the observed patterns have been studied by 2D FTs of those images [see Figs. 3(b), 3(d), and 3(f)]: depending on the energy, the FT of the standing waves shows intense maxima from either three or five pairs of points superimposed on a faint circular background attributed to scattering with randomly distributed pointlike defects. If the 2D maps are recorded at increasing distances from the molecular edge, the intensity of these spots decreases, so they can be attributed to scattering of surface-state electrons with TCNQ molecules. The momentum transfer values parallel to the edge for the observed maxima, $\Delta k_\parallel$, are equally spaced by 1.8 nm^{-1} for all the energies investigated. Comparison between the 2D maps and the energy resolved $dI/dV(k_\perp, E)$ demonstrates that for each energy, the perpendicular momenta for the three subbands in Fig. 3(g) correspond to the projections of the Δk vectors at which the maxima are found in the 2D map over the perpendicular axis.

The quantization of the parallel momentum transfer, $\Delta k_{\parallel,n} = nG$, is strongly reminiscent of the Laue condition for diffraction of a 2D wave with a 1D crystal. The reciprocal space of the 1D TCNQ edge consists of a regular array of straight lines perpendicular to the edge with a spacing of $2\pi/a = 1.8$ nm^{-1} [see Fig. 1(b)], in perfect agreement with the value of G within experimental error. From that point of view, our experimental results are comparable to a low-energy electron diffraction experiment in which the probe beam is composed of bound 2D electrons instead of free 3D electrons. One important

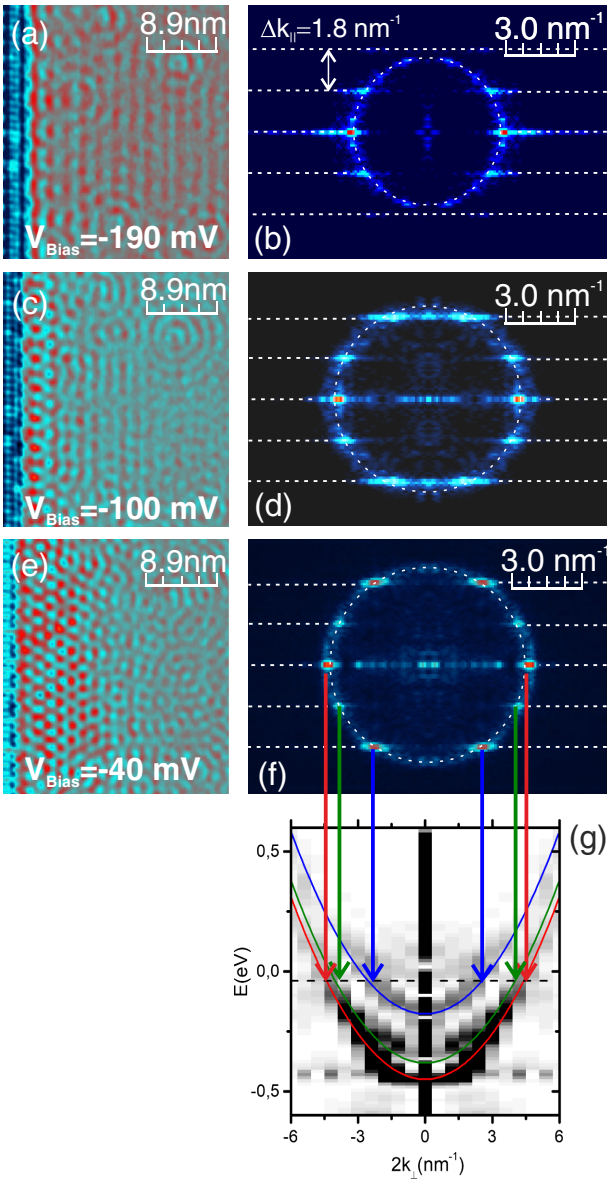

FIG. 3. $dI/dV(x,y)|_E$ maps recorded with the lock-in amplifier at different bias voltages (a), (c), and (e) and their corresponding symmetrized 2D FT images (b), (d), and (f). All the maps have been recorded with the same modulation of 14m V, and current setpoints of 1.2 nA, 1.2 nA, and 0.3 nA, respectively. The 2D FTs have been performed in the molecule-free areas close to the molecular edges. At the constant-energy circles arising from scattering with different types of surface defects (white dotted circles), some points appear with a rather large intensity, being equally spaced in $\Delta k_\parallel$ (white dotted lines). (g) The projection onto the $\Delta k_\perp$ axis of the high-intensity points in the 2D FTs correspond to the momenta of the three parabolas found in Fig. 2.

difference, however, is the direction of the incident electrons: while in standard diffraction techniques the incidence angle is chosen by the experimentalist, in our results surface-state electrons will arrive at the TCNQ edge from every possible direction in the half-plane not occupied by the island [Figs. 4(a)–4(c), top panel]. As can be observed

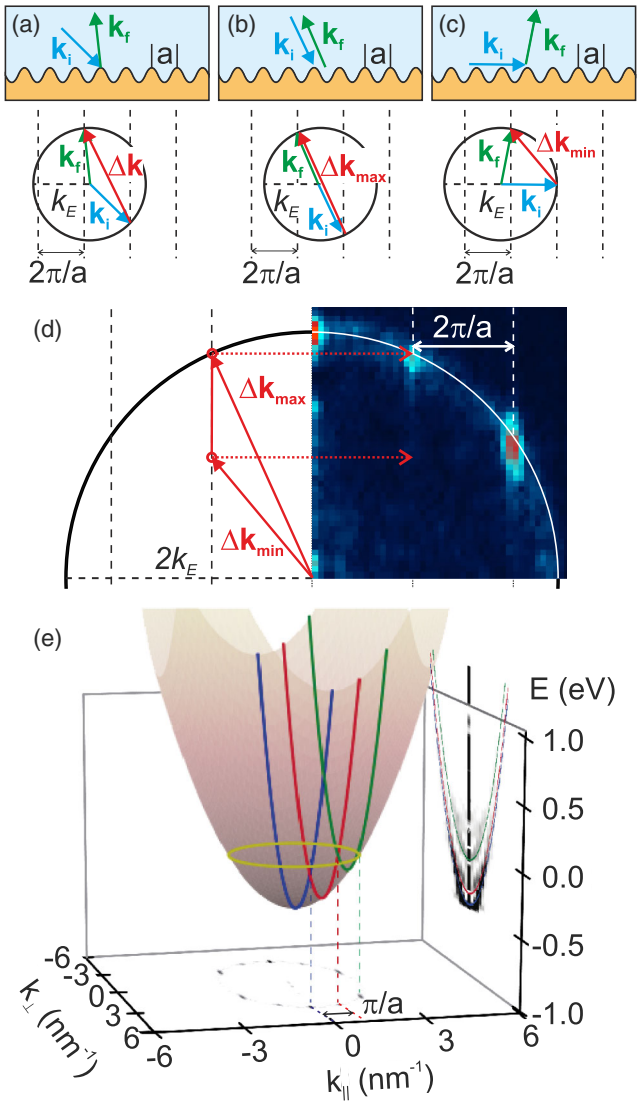

FIG. 4. (a)–(c) Scattering geometry for three possible incidence angles of the incoming electron, calculated for an energy of −40 meV and $n = -1$ in the Laue condition. *Top panel:* Real-space representation of the scattering process [orange area corresponds to the TCNQ edge, light cyan area to bare Cu(111)]. Blue (green) vectors represent the momentum of the incident (scattered) electron. *Bottom panels:* Ewald-sphere visualization of the scattering events (vertical dotted lines correspond to the reciprocal space of the TCNQ edge; solid circles represent the constant-energy surfaces). Momentum transfer vectors associated with these scattering processes are also drawn in red. (b) Extremal backscattering configuration. (c) Limiting grazing incidence case. (d) Momentum-transfer space derived from the previous analysis compared to the experimental $dI/dV(x,y)|_E$ maps at −40 meV, showing that the vectors contributing to the standing waves are those corresponding to backscattering processes. (e) Origin of the discrete subbands as intersections between the 2D surface-state paraboloid and the constant $k_\parallel$ planes originating from the Laue and backscattering conditions ($k_{\parallel,n} = nG/2$).

in Figs. 4(a)–4(c), each incidence angle will lead to a different momentum transfer vector ($\Delta\mathbf{k}$), which can be calculated by using the Ewald sphere construction to take into consideration diffraction and energy conservation [lower panels in Fig. 4(a)–4(c)]. All the possible $\Delta\mathbf{k}$ vectors have the same parallel component as determined by the Laue condition (nG), but the modulus can change from a maximum value of $2k_E$ for the backscattering configuration [Fig. 4(b)] to a minimum value for grazing incidence or grazing direction of the scattered electron [Fig. 4(c)]. Each incidence direction should thus lead to a standing wave pattern with a different periodicity perpendicular to the TCNQ edge, and the superposition of all such waves should blur out the observation of the diffraction subbands. Notice, thus, that diffraction is not enough to explain the discretization of the band structure, as it only leads to the quantization of the momentum transfer, but not of the momentum itself.

However, when comparing the experimental 2D FT with the continuous distribution of momentum transfer values expected from our previous analysis [Fig. 4(d)], we observe that the intensity is strongly localized at the $2k_E$ circle, which implies that out of all the possible scattering geometries, the backscattering processes make the largest contribution to the observed standing wave pattern. Notice that, taking into consideration both the Laue condition for Bragg diffraction ($\Delta k_{\parallel,n} = k_{\parallel,f} - k_{\parallel,i} = nG$) and the backscattering condition ($k_{\parallel,i} = -k_{\parallel,f}$), we must conclude that the DOS of the sample is dominated by electrons for which the parallel component of both the incoming and outgoing momenta is quantized in units of $G/2$. The electronic structure of the Cu(111) surface state near the edges of TCNQ islands is thus discretized by this process, and the original surface-state paraboloid becomes a discrete collection of subbands obtained from the intersection of the paraboloid with a set of equally spaced planes of constant $k_\parallel = nG/2$ [see Fig. 4(e)]. The bottoms of these subbands are shifted upwards in energy by $\hbar^2/2m^*(nG/2)^2 = \hbar^2/2m^*(n\pi/a)^2$ with respect to the bottom of the paraboloid. These shifts become very large for a short periodicity of the scatterers. For example, for a periodicity of the order of the interatomic distances (∼0.3 nm, such as the one at bare step edges), the bottom of the first subband is calculated to be 9 eV above the bottom of the band, rendering this effect unobservable. Thus, our observation is only possible because of the large periodicity of the TCNQ edge.

To summarize, the diffraction of 2D electrons with a 1D periodic array of molecular scatterers leads to the quantization of the momentum parallel to the edge in half-integer units of the reciprocal space vector of the edge G, and thus leads to the existence of discrete subbands of the copper surface-state electrons close to the corrugated edges of TCNQ islands even without full quantum confinement.

While we have demonstrated this effect for a 2D surface state interacting with a corrugated 1D edge, a similar effect can also be envisioned for 3D bulk electrons interacting with a properly engineered 2D superlattice at the surface, thereby creating a layer of electronic states with a modified DOS of thickness of the order of the electronic coherence length. It is important to realize that the splitting of the 2D surface-state band into a set of discrete 1D parabolic subbands should modify the constant DOS of the surface state into a set of van Hove singularities at the energies of the bottom of the subbands. Since these energies are in turn determined by the periodicity of the scatterers, we conclude that Bragg-diffraction discretization offers a new avenue to tailor the DOS at the Fermi level, and thus the physical properties of materials, from the superconducting transition temperature to their thermal stability.

The authors acknowledge financial support from the Spanish Ministry for Economy and Competitiveness [Grants No. FIS2015-67367-C2-1-P, No. FIS2015-72482-EXP, No. FIS2016-78591-C3-1-R, and the María de Maeztu Programme for Units of Excellence in R&D (No. MDM-2014-0377)], the regional government of Comunidad de Madrid (Grants No. S2013/MIT-3007, No. S2013/MIT-2850, and No. S2018/NMT-4321), Universidad Autónoma de Madrid (UAM/48), and IMDEA Nanoscience. IMDEA Nanociencia acknowledges support from the Severo Ochoa Programme for Centres of Excellence in R&D (MINECO, Grant No. SEV-2016-0686).

*roberto.otero@uam.es

[1] C. Cohen-Tannoudji, B. Diu, and F. Laloë, *Quantum Mechanics* (Wiley, New York, 1997).
[2] P. Harrison, *Quantum Wells, Wires and Dots* (Wiley, New York, 2005).
[3] S. Qin, J. Kim, Q. Niu, and C.-K. Shih, Science **324**, 1314 (2009).
[4] R. Otero, A. L. Vázquez de Parga, and R. Miranda, Phys. Rev. B **66**, 115401 (2002).
[5] V. Yeh, L. Berbil-Bautista, C. Z. Wang, K. M. Ho, and M. C. Tringides, Phys. Rev. Lett. **85**, 5158 (2000).
[6] W. B. Su, S. H. Chang, W. B. Jian, C. S. Chang, L. J. Chen, and T. T. Tsong, Phys. Rev. Lett. **86**, 5116 (2001).
[7] F. Calleja, M. C. G. Passeggi, J. J. Hinarejos, A. L. Vázquez de Parga, and R. Miranda, Phys. Rev. Lett. **97**, 186104 (2006).
[8] A. Cebollada, R. Miranda, C. M. Schneider, P. Schuster, and J. Kirschner, J. Magn. Magn. Mater. **102**, 25 (1991).
[9] J. E. Ortega and F. J. Himpsel, Phys. Rev. Lett. **69**, 844 (1992).
[10] M. F. Crommie, C. P. Lutz, and D. M. Eigler, Nature (London) **363**, 524 (1993).
[11] Y. Hasegawa and P. Avouris, Phys. Rev. Lett. **71**, 1071 (1993).
[12] M. F. Crommie, C. P. Lutz, and D. M. Eigler, Science **262**, 218 (1993).
[13] P. Avouris and I.-W. Lyo, Science **264**, 942 (1994).
[14] L. Bürgi, H. Brune, O. Jeandupeux, and K. Kern, J. Electron Spectrosc. Relat. Phenom. **109**, 33 (2000).
[15] D. Stradi, B. Borca, S. Barja, M. Garnica, C. Diaz, J. M. Rodriguez-Garcia, M. Alcami, A. L. Vazquez de Parga, R. Miranda, and F. Martin, RSC Adv. **6**, 15071 (2016).
[16] M. M. Kamna, T. M. Graham, J. C. Love, and P. S. Weiss, Surf. Sci. **419**, 12 (1998).
[17] L. Gross, F. Moresco, L. Savio, A. Gourdon, C. Joachim, and K.-H. Rieder, Phys. Rev. Lett. **93**, 056103 (2004).
[18] Y. Pennec, W. Auwärter, A. Schiffrin, A. Weber-Bargioni, A. Riemann, and J. V. Barth, Nat. Nanotechnol. **2**, 99 (2007).
[19] J. Lobo-Checa, M. Matena, K. Müller, J. H. Dil, F. Meier, L. H. Gade, T. A. Jung, and M. Stöhr, Science **325**, 300 (2009).
[20] J. Wyrick, D.-H. Kim, D. Sun, Z. Cheng, W. Lu, Y. Zhu, K. Berland, Y. S. Kim, E. Rotenberg, M. Luo, P. Hyldgaard, T. L. Einstein, and L. Bartels, Nano Lett. **11**, 2944 (2011).